Colloid and Interface Science Communications 50 (2022) 100669

Contents lists available at ScienceDirect

Colloid and Interface Science Communications

journal homepage: www.elsevier.com/locate/colcom

Rapid Communication

Choice of the functional monomer of molecularly imprinted polymers: Does it rely on strong acid-base or hydrogen bonding interactions?

Merymene Boukadida [a,b], Amira Anene [c], Najeh Jaoued-Grayaa [c], Yves Chevalier [a,*], Souhaira Hbaieb [b,*]

[a] Laboratoire d'Automatique, de Génie des Procédés et de Génie Pharmaceutique, Université de Lyon 1, UMR 5007 CNRS, 69622 Villeurbanne Cedex, France
[b] Laboratoire de Recherche: Caractérisations, Applications et Modélisation de Matériaux, Université de Tunis El Manar, Faculté des Sciences de Tunis, Campus universitaire El Manar, Tunisia
[c] Unité Spécialisée de développement des techniques analytiques, Institut National de Recherche et d'Analyse Physico-chimique, Biotechpole Sidi-Thabet, 2020 Ariana, Tunisia

ARTICLE INFO

Keywords:
Molecularly imprinted polymer
Hydrogen bonding
Histamine
Molecular recognition

ABSTRACT

The choice of the functional monomer is a key point in the design of molecularly imprinted polymers (MIPs) because its directional interactions with template molecules are required to form molecular imprints acting as selective recognition sites for adsorption. Methacrylic acid (MAA) has very often been employed as a functional monomer for imprinting basic template molecules. Strong acid-base interactions lead to H^+ transfer and weak hydrogen bonding between the products of the acid-base reaction. The weakly acidic acrylamide (AA) has shown stronger hydrogen-bonding interactions with histamine (HA) than MAA. Interactions between HA and the functional monomers have been investigated by means of ^{1}H NMR spectroscopy yielding the stoichiometry and complexation constants of their complex species. Adsorption isotherms of HA to both MAA- and AA-based MIPs and their modeling showed a higher selective binding of HA to the AA-based MIP.

1. Introduction

Molecular imprinting technology has become a widely used approach for creating polymeric adsorbents having preset selective recognition sites. Molecularly imprinted polymers (MIPs) are solid materials having 'cavities' with well-positioned functional groups that act as selective molecular recognition sites for the adsorption of target molecules [1]. The molecular imprints are built by a templated copolymerization of a functional monomer that strongly interacts with the template molecule and a large amount of cross-linking agent that brings rigidity to the material. Removal of the template by extraction leaves the molecular imprints having the memory of the shape and position of functional groups of the template molecule. The idea of selective binding coming from the shape of a cavity is suggested by many artistic sketches shown in the literature [1,2,3]. Such cavities have never been observed. The origin of selective binding better stands in the right position of functional groups for optimum directional interaction with the template molecule and possible binding to several interaction sites within the molecular imprint [4]. Therefore, a cavity having shape-memory is not enough, a functional monomer is needed. Within this framework, strong interactions between the functional monomer and the template are a priori favored. Although the interactions that actually matter are those with the polymer material and the template, the functional monomer is usually selected on the basis of its interactions with the template. The idea of a pre-polymerization complex between monomer and template molecule has been put forward [5,6].

Methacrylic acid (MAA) is the most often used functional monomer. Indeed, it is an acid that may strongly interact with bases and it is a hydrogen-bonding donor. MIPs based on MAA as functional monomer and ethylene glycol dimethacrylate (EGDMA) as cross-linking agent are by far the mostly investigated materials, so that a specific chapter has been devoted to this material in the book by Selergren [7]. All reported instances claim for selective molecular imprints as inferred from the difference of adsorption behavior of MIP and non-imprinted polymer (NIP) materials. In the case of a basic template molecule such as an amine, the interaction with MAA is presumed strong. However, an acid-base chemical reaction occurs where the hydrogen atom of the carboxylic acid is transferred as an H^+ ion to the amino group of the template molecule (Fig. 1). The chemical species that interact actually are the products of the acid-base reaction which are a weak base (carboxylate

* Corresponding authors.
E-mail addresses: yves.chevalier@univ-lyon1.fr (Y. Chevalier), souhaira.hbaieb@fst.utm.tn (S. Hbaieb).

https://doi.org/10.1016/j.colcom.2022.100669
Received 5 June 2022; Received in revised form 23 August 2022; Accepted 22 September 2022

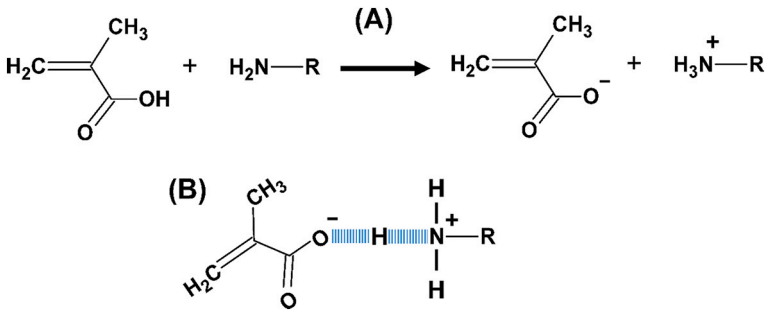

Fig. 1. (A) Acid-base reaction of MAA and an amine, and (B) the subsequent possible hydrogen bonds that may operate a selective recognition.

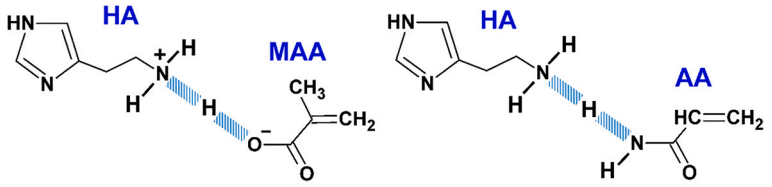

Fig. 2. Hydrogen-bonded complexes of histamine (HA) and either methacrylic acid (MAA) or acrylamide (AA).

anion) and a weak acid (ammonium cation). Interactions through hydrogen bonds are still possible; but they are much weaker than expected on the basis of the strengths of the acid (MAA) and the base (amine). The acid-base reaction yields ionic species of opposite charges that may bind through electrostatic interactions. However, electrostatic interactions are neither directional nor specific, so that they cannot achieve selective binding. The ammonium cation possibly bound to the carboxylate anion of the MIP by electrostatic interactions can be ion-exchanged with any cation (e.g. Na^+) present in the liquid medium.

The most efficient directional interaction responsible for selectivity is the hydrogen bond. The numerous examples in nature advocate this fact: RNA hybridization, secondary structure of proteins, collagen fibers… The hydrogen bond is a type of acid-base interaction where the hydrogen atom is shared by the H-donor and the H-acceptor. In case of too strong acid-base interaction, a full H^+ transfer takes place instead. Therefore, MAA may not be the best choice as a functional monomer for the preparation of MIPs selectively binding amines or other strongly basic species. A functional monomer having weakly acidic groups may be better. The present study selected acrylamide (AA) as such weakly acidic functional monomer. Acrylamide monomers have been shown efficient in providing selectivity to the MIPs materials toward both carboxylic anion targets [8] and more complex species such as proteins [9]. MIPs based on AA and MAA are compared for their ability to selectively bind histamine (HA) as a model basic template [10,11,12]. Histamine has three amino groups; only two of their ammonium forms have been given a p*K*a value. The imidazolium is more acidic (p*K*a = 5.94) than the primary ammonium (p*K*a = 9.80) [13], so that the primary amine of histamine predominantly reacts with methacrylic acid. On this basis, hydrogen bonding of HA and MAA takes place between the histamine under the protonated form at its primary amine and the methacrylate anion. The most acidic group of AA is the NH_2 of the primary amide group (p*K*a is 7.9 [14]). It can bind to the most basic group of histamine under its neutral form, namely the primary amino group. Tentative sketches of hydrogen bonding interaction of HA with AA and MAA are given in Fig. 2. Hydrogen bonding interactions are presently considered because they are the strongest in the hierarchy of intermolecular interactions. Obviously, other types of interactions may also operate; for instance, anion-π interactions [15] between the MAA carboxylate anion and the aromatic imidazole ring that has 6 π electrons. Such other interactions are presently ignored for the sake of simplicity because this shortcut does not interfere with the present general approach and the conclusions.

Table 1
List of abbreviations for widely used products.

Compound/Material	Abbreviation
Histamine	HA
Acrylamide	AA
Methacrylic acid	MAA
MAA-based MIP	MIP@MAA
MAA-based NIP	NIP@MAA
AA-based MIP	MIP@AA
AA-based NIP	NIP@AA

MAA and AA were then tested to assess their potential rebinding characteristics under the same conditions, hence, the effect of the strength of the interactions in the pre-polymerization complex on the performance of the final imprinted material. To increase the efficiency of non-covalently imprinted systems, a deeper knowledge of the molecular mechanisms controlling complex formation in the pre-polymerization solution is necessary. A ^1H NMR study was used to investigate the complexation process in the pre-polymerization mixtures [16]. As observed, AA has strong hydrogen bonding interactions with HA when compared to MAA. The results of NMR analysis of both systems now allow for a more broad view of the complexation occurrences in the pre-polymerization solution, and NMR investigations of monomer–template complexation constants can predict MIP binding capacities and their impact on the recognition properties of the MIPs formed from these systems [17]. The polymerization process used was radical polymerization using azobis(isobutyronitrile) (AIBN) as the initiator and acetonitrile as the solvent. The non-imprinted polymers (NIPs) are prepared similarly to imprinted polymers without HA molecules.

2. Experimental

2.1. Materials and reagents

All chemicals and solvents used were purchased from Sigma-Aldrich. Aerosil 200 fumed silica was used as a solid support. Deuterium oxide and DMSO-d_6 (99.9%) were used as solvents for NMR analyses. Deionized water of resistivity 18 MΩ•cm was used throughout the whole study.

Table 1 below includes the list of acronyms for the products required

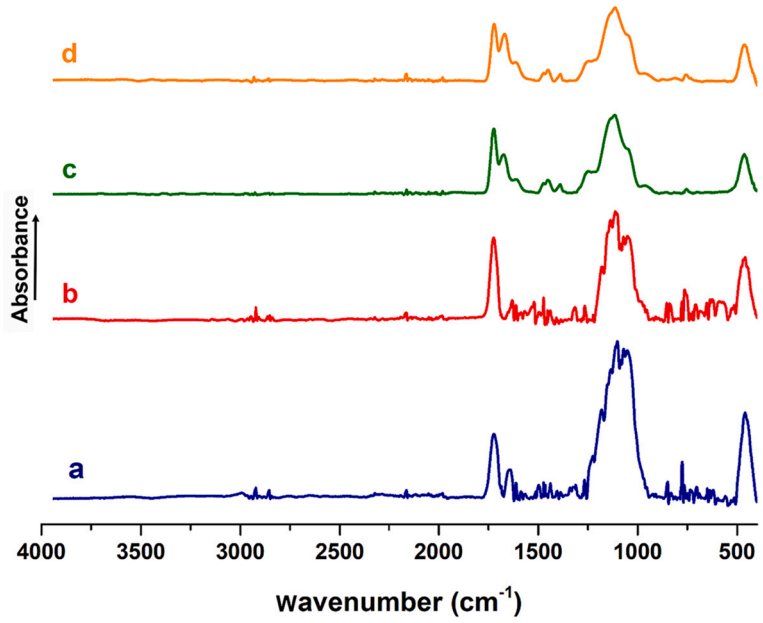

Fig. 3. IR spectra of MIP@MAA (a), NIP@MAA (b), MIP@AA (c) and NIP@AA (d).

to carry out this work:

2.2. Synthesis of the imprinted materials

The synthesis was adapted from previous works [18,19,20]. The modification of the silica was carried out in the first step. The methacryloyloxypropyltriethoxysilane (APTES-MA) was synthesized by mixing a toluene solution (60 mL) of (3-aminopropyl)triethoxysilane (2.5 mL, 14.32 mmol) and triethylamine (3 mL, 22.22 mmol) and a toluene solution (40 mL) of methacryloyl chloride (2.5 mL, 25.58 mmol); the reaction mixture was stirred at room temperature for 48 h before being filtered. The filtrate was dried under reduced pressure and purified by chromatography on silica gel with (80/20: hexane/ethyl acetate) as the eluent to provide APTES-MA as a yellowish oil product. Thereafter, 5 g of activated silica was dispersed in 150 mL of toluene containing 5 mL of N,N-diisopropylethylamine, and 3 g (12.13 mmol) of APTES-MA in 50 mL of toluene was added. The mixture was stirred at 120 °C for 24 h, then filtered and washed with THF. The modified silica SiO_2(APTES-MA) material was dried in an oven at 60 °C. The two MIPs were made via radical polymerization: 500 mg of SiO_2(APTES-MA) was mixed with 1 mmol of HA in 20 mL of acetonitrile at 80 °C. The reaction medium was de-oxygenated by bubbling nitrogen gas for 20 min. 8 mmol of the appropriate monomer (MAA or AA), 8 mmol of the cross-linking agent EGDMA and 0.2 mmol of the initiator AIBN were then added. Polymerization lasted for 1 h. The obtained materials were extracted in a Soxhlet system with methanol for 72 h and subsequently washed with water for 72 h to remove the template molecules. The final materials were dried in a vacuum oven for 24 h. Non-imprinted polymers were synthesized under identical conditions as MIPs without the HA molecule.

2.3. Characterization methods

IR absorption spectra were collected using an ATR mode Bruker IFS 55 Equinox FTIR spectrometer. Thermogravimetric analyses (TGA) were carried out using a TG209F1 Netzsch instrument in the temperature range of 25–1000 °C at a heating rate of 10 °C•min^{-1} in a nitrogen gas flow.

The BET technique was used to quantify the entire adsorption and desorption isotherms of nitrogen gas at 77 K using a Micromeritics ASAP2020 device, yielding the specific surface area and mesoporosity. Prior to nitrogen adsorption tests, the materials were dried at 150 °C. Fitting the BET theoretical isotherm to the experimental adsorption branch between the relative pressures p/p_0 0.05 and 0.3 yielded the BET specific area. The BJH approach was used to calculate the distribution of porous volume in the mesopores ranges from the experimental desorption branch.

Transmission Electron Microscopy (TEM) images were taken using a Philips CM120 microscope operated at 80 kV acceleration voltage at the "Centre Technologique des Microstructures" (CTμ) facility (http://microscopies.univ-lyon1.fr/) of the University of Lyon 1. A 0.2% aqueous dispersion drop was put on a Formvar film-coated grid and dried in the open air before observation by TEM.

2.4. NMR analyses

^{1}H NMR spectra were recorded on a Bruker Avance III 500.13 ultra shield Plus spectrometer at 25 °C. Chemical shifts are referenced to the DMSO-d_6 solvent signal and given with respect to TMS. Job plot analysis was used to determine complex stoichiometry as well as complexation constants. A range of solutions containing different proportions of HA and monomer while keeping the total concentration of the mixture constant (0.026 M); they are characterized by a mole fraction of histamine, r, varying from 0 to 1. The response observed in NMR is the difference in the chemical shift ($\Delta\delta$) between the free and complexed forms. The stoichiometry of the complex is graphically visualized from the maximum of $r\Delta\delta$ for the lines of histamine and the maximum of $(1-r)\Delta\delta$ for the lines of the monomer: a maximum at $r = 0.5$ indicates a 1:1 stoichiometry. However, the Job plots were calculated from the basic equations describing the association equilibrium and materials balance (SI file) and fitted to the experimental data, so that the present method is not the original Job method [21,22], but an exact modeling of the NMR chemical shifts of a series of mixtures prepared using the Job mixing scheme.

2.5. Adsorption experiments

30 mg of MIPs or NIPs were dispersed in 5 mL of HA aqueous solution in the concentration range from 5 ppm to 300 ppm. The mixtures were kept at room temperature for 20 min to achieve equilibrium before being

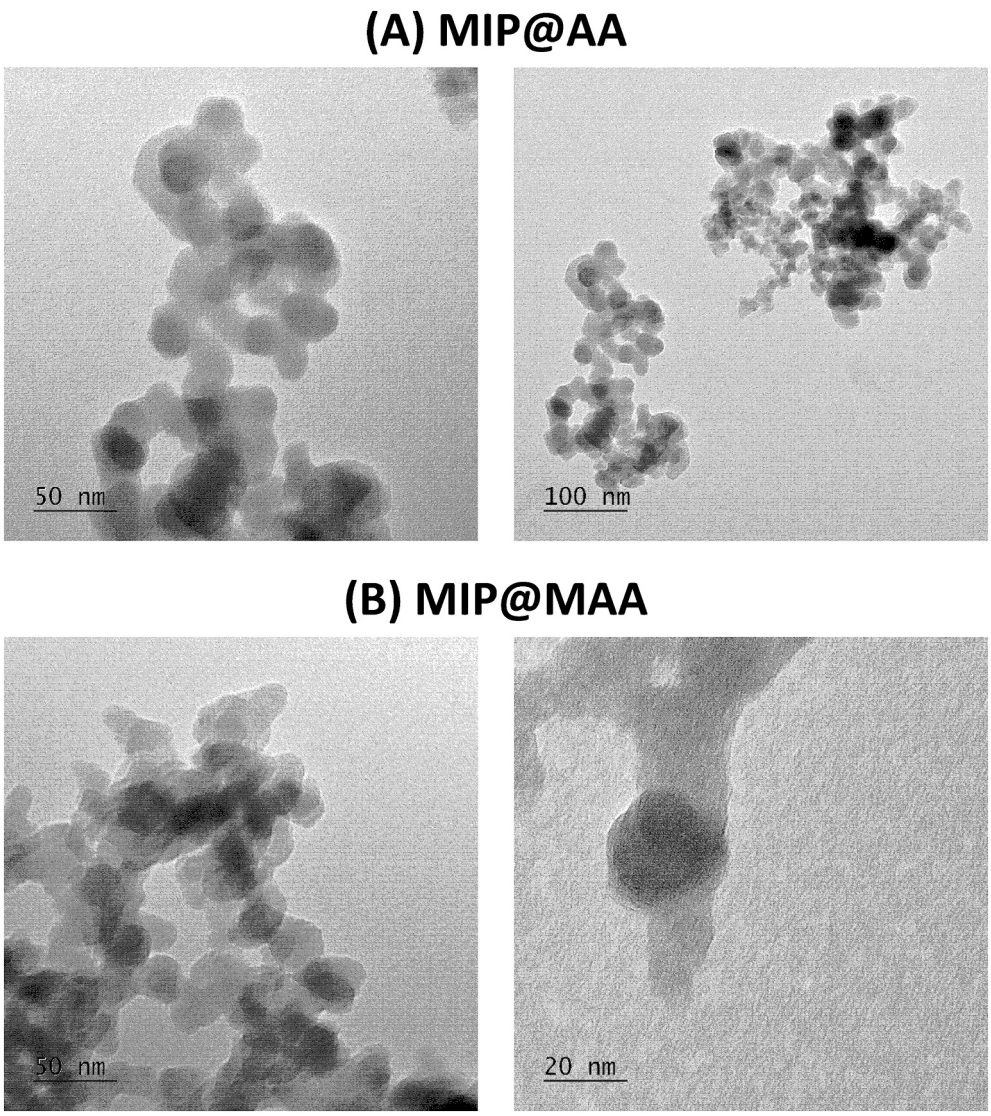

Fig. 4. TEM images MIP@AA (A) and MIP@MAA (B) at two magnifications.

centrifuged at 10000 rpm for 10 min. The residual concentration of HA in the supernatant was measured using LC-MS [12,23] (SI file). The peak of the molecular ion of HA at m/z = 112 g•mol^{-1} was used for quantification.

3. Results and discussion

3.1. Synthesis and characterization of MIPs and NIPs materials

The surface imprinting approach [24] was used. The fumed silica support has been selected for its optimal porosity allowing accessibility to the MIP surface during adsorption experiments. The modified silica was characterized by thermogravimetric analyses and elemental analyses of carbon and nitrogen. The grafting density of APTES-MA onto silica was 6.2–6.4 mol•m^{-2} (section S1 of the SI file).

HA-imprinted polymers were synthesized by radical polymerization in acetonitrile using two types of monomers: MAA and AA, EGDMA as a cross-linking agent and the radical initiator AIBN. Similar polymerization conditions were used to produce NIPs, except that the HA molecule was absent during the polymerization process. The MIP and NIP materials are abbreviated as MIP@MAA, NIP@MAA, MIP@AA and NIP@AA.

IR spectra showed that HA has been completely eliminated from MIP materials during the extraction process since there was no visible difference between the spectra of MIP and NIP. The IR spectra of MIP and NIP materials (Fig. 3) revealed an absorption band at 1760 cm^{-1} for materials synthesized with the MAA monomer and at 1640 cm^{-1} for materials synthesized with the AA monomer, which corresponded to vibrations of elongation relative to C═O bonds. Strong peaks at 1100 cm^{-1} corresponded to the Si–O–Si elongation vibrations.

TGA was then used to make quantitative determinations of the polymer content (Section S2 in SI file). TGA records of MIPs and NIPs were identical (Fig. S3). The polymer contents were 53% for MAA-based MIP and NIP, and 68% for AA-based MIP and NIP (Table S2). The origin of the larger polymer content of AA-based materials is the higher reactivity of AA in free radical polymerization. Thus, the propagation rate constants measured in aqueous solution at 80 °C are 16,544 L•mol^{-1}•s^{-1} for non-ionized MAA and 1158 L•mol^{-1}•s^{-1} for fully ionized MAA [25], whereas it is 145,000 L•mol^{-1}•s^{-1} for AA (value extrapolated to 80 °C by an Arrhenius-type plot of experimental data between 5 °C and 70 °C [26]).

TEM images of the MIP@AA and MIP@MAA materials revealed small aggregates of primary particles with a narrow particle size distribution centered around 20 nm (Fig. 4). MIP@AA and MIP@MAA are nanocomposite materials made of silica particles coated with a thin layer of MIP. Image analysis of the TEM pictures gave the primary particles average size of 26.8 ± 1.2 nm with a standard deviation SD =

3.4 nm for MIP@AA and 27.7 ± 1.2 nm with an *SD* of 2.1 nm for MIP@MAA.

BET measurements of nitrogen gas adsorption at 77 K were used to determine the materials specific surface area and porosity. The HA imprinted polymers synthesized with MAA and AA monomers exhibited "type II" isotherms [27] (Fig. S4 in SI file) showing a weak hysteresis between the adsorption and desorption branches. The specific surface area was MIP@MAA 102 $m^2 \bullet g^{-1}$ for MIP@MAA and 31 $m^2 \bullet g^{-1}$ for MIP@AA. Mesopores size distribution from BJH analysis of the desorption branch revealed a low pore volume for MIP@AA with average pore sizes of 35 nm for MIP@AA and 44.4 nm for MIP@MAA. The total mesoporous volume for the MIP@MAA was 0.66 $cm^3 \bullet g^{-1}$ (66%) and 0.1 $cm^3 \bullet g^{-1}$ (10%) for the MIP@AA, indicating that the material synthesized with MAA is more porous than that synthesized with AA, which is consistent with the higher value of specific surface area of MIP@MAA.

Assuming a perfect core shell morphology of the primary particle with a spherical core of silica coated by a shell of MIP material, the thickness t of the polymer coating would be given by Eq. 1

$$t = \frac{3}{\rho A_{sp}} - \frac{3}{\rho_{core} A_{sp,core}} \quad (1)$$

where ρ and A_{sp} are the density and specific area of the polymer-coated primary particles, $\rho_{core} = 2.0$ g•cm^{-3} and $A_{sp,core} = 200$ $m^2 \bullet g^{-1}$ are the density and specific area of the silica core. The density of the MIP material is taken as $\rho = 1$ g•cm^{-3} for the calculation of an order of magnitude of t. The thicknesses of polymer coatings are 22 nm for MIP@MAA and 90 nm for MIP@AA. The TEM pictures did not show such large particles and there is the specific areas of the MIP materials were much lower than that of the bare fumed silica. These features rule out the core-shell morphology. The TEM pictures showed that the polymer material filled the porosity of fumed silica and bridged together the primary silica particles. These effects were less for the MIP@MAA that had a lesser polymer content, so that polymerization left more porosity as shown by the BJH calculation of the mesoporous volume. The morphologies of the MIP@MAA and MIP@AA materials were slightly different. A correct comparison of their adsorption behavior was therefore made on the basis of the adsorbed amount per unit surface area (Q was expressed in mol•m^{-2}).

3.2. NMR studies

The choice of the functional monomer is often made on the basis of the strength of the specific interactions between the template and functional monomer molecules [17]. Indeed, it is believed that a pre-polymerization complex forms in solution before polymerization. Such interactions have been investigated using ^{1}H NMR spectroscopy.

The formation of complexes between MAA or AA with HA in solution rely on hydrogen bonds. The difference of chemical shifts between the mixtures and the pure compounds were measured using a mixing scheme corresponding to a Job method [28,29]. For AA the chemical species that undergoes hydrogen bonds interaction with HA is AA itself. This is different for MAA because MAA reacts first with HA by an acid-base reaction; the species that are actually interacting are the products of the reaction, namely the methacrylate anion and the protonated HA (Fig. 2). The tetramethylammonium methacrylate salt and the HA hydrochloride were taken as the reference pure species. The extended details of the data manipulation are given in SI file. The Job plots $r\,\Delta\delta = f(r)$ and $(1 - r)\,\Delta\delta = f(1 - r)$ provide graphical estimates of the stoichiometry of the pre-polymerization complex. The maximum at $r = 0.5$ indicated a 1:1 stoichiometry for both cases. The quantitative determination of the complexation constant was done by an exact calculation of the Job plots using the definition of the complexation constant (Eq. S5) and material balance of HA and monomer (Eqs. S6 and S7) (see SI file). The 1:1 model accurately fitted to the experimental data (Figs. S7 to S10), confirming the 1:1 stoichiometry inferred from the maximum in the Job plots, and giving the complexation constants as $K = 400$ for HA-MAA and $K = 1000$ for HA-AA. The complexation of HA with AA is stronger than with MAA, although MAA is a stronger acid than AA because the hydrogen-bonding interactions that matter are those with the products of the acid-base reaction of MAA with HA. In the framework of the pre-polymerization complex, this result suggests that AA as a monomer is more suitable for the recognition of HA in molecularly imprinted polymers.

3.3. Adsorption experiments

Binding experiments were then carried out to evaluate the recognition properties of MIP@AA and MIP@MAA toward HA. The thermodynamic equilibrium between adsorbed and free HA molecules is expressed by "adsorption isotherms," which relate the equilibrium between surface concentrations Q(µmol•m^{-2}) and the concentration in solution C(mol•L^{-1}). Adsorption isotherms were measured after an equilibrium time of 40 min (equilibrium was reached within less than 20 min). They were used to calculate the binding capacity and assess the binding behavior of the prepared materials. The binding model considers two simultaneous adsorption phenomena: selective adsorption of HA to molecular imprints and non-selective adsorption off the molecular imprints. Molecular imprints are well-defined sites when adsorbed molecules are localized; it is described by the Langmuir model. HA molecules adsorbed besides the molecular imprints can freely diffuse on the MIP surface. Such adsorption is described by the Volmer model for non-localized adsorption of mobile molecules. The combination of the two has been called the Langmuir–Volmer model [30].

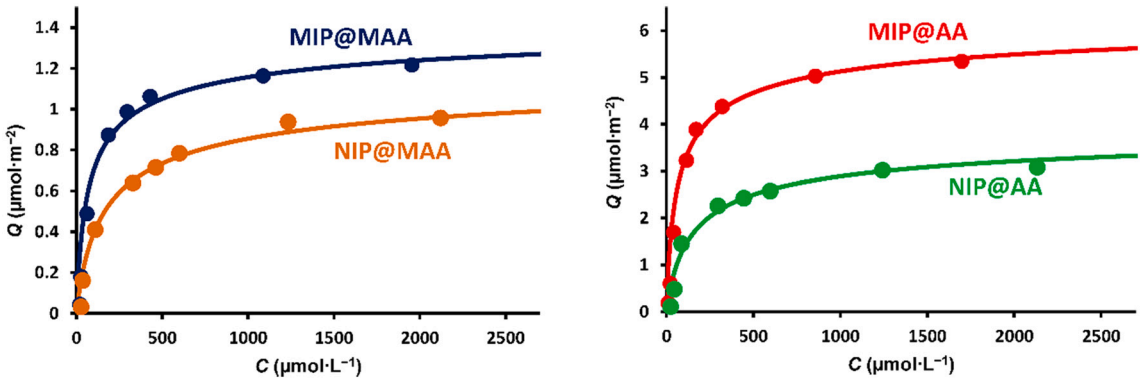

Fig. 5. Adsorption isotherms and best non-linear fits of the adsorption models to experimental HA adsorption onto MIP@AA and NIP@AA, MIP@MAA and NIP@MAA.

Table 2
Parameters of the Langmuir–Volmer, and Volmer models fitting to HA experimental adsorption isotherms of MIP@AA and NIP@AA, MIP@MAA and NIP@MAA at 298 K and pH 5.5.

	$Q_{max,s}$ (μmol•m^{-2})	K_s	log(K_s)	$Q_{max,ns}$ (μmol•m^{-2})	K_{ns}	log(K_{ns})
MIP@AA	0.163	24,900	4.39	7.55	13,315	4.12
NIP@AA				5	5407	3.73
MIP@MAA	0.085	15,490	4.19	1.65	12,315	4.09
NIP@MAA				1.5	5000	3.69

3.3.1. Interpretation using the Langmuir-Volmer model

The following thermodynamic models were used to describe the adsorption of HA to MIP@AA, NIP@AA, MIP@MAA and NIP@MAA:

3.3.1.1. Langmuir model

$$Q_s = Q_{max,s}\frac{K_s\, C}{1 + K_s\, C} \tag{2}$$

where Q_s (μmol•m^{-2}) is the adsorbed quantity at equilibrium, $Q_{max,s}$ (μmol•m^{-2}) is the maximum adsorption capacity for specific sites, C (μmol•L^{-1}) is the concentration of HA at equilibrium, and K_s is the binding constant for specific sites [31].

3.3.1.2. Volmer model

$$C_e = \frac{1}{K_{ns}}\frac{\theta}{1-\theta}e^{\frac{\theta}{1-\theta}} \tag{3}$$

where $\theta = Q/Q_{max,ns}$ is the coverage and K_{ns} is the binding constant for non-specific adsorption [32].

The Volmer model was used for the non-selective part of adsorption to MIP and for the adsorption to NIP.

The theoretical isotherms were fitted to the experimental data by non-linear regression. The outcomes are binding constants and maximum coverage for each adsorption process. The parameters for adsorption to MIPs are K_s, $Q_{max,s}$, K_{ns}, and $Q_{max,ns}$ for specific (subscript "s") and non-specific (subscript "ns") adsorption. Adsorption to NIP is described by the two parameters K_{ns} and $Q_{max,ns}$. The best fit was found by minimizing the absolute relative error (*ARE,* Eq. 4).

$$ARE = \frac{1}{(N-p)}\sum_{i=1}^{N}\left|Q_{exp} - Q_{calc}\right| \tag{4}$$

where N is the number of data points and p is the number of adjustable parameters.

Fig. 5 shows the experimental adsorption isotherms at 298 K at pH 5.5 for MIP@AA, NIP@AA, MIP@MAA, and NIP@MAA, as well as the best fit of the appropriate model. Table 2 lists the thermodynamic parameters.

As shown in Fig. 5, the predicted adsorption isotherms fit the experimental data quite well in all cases. The adsorbed quantities to MIP are higher than to NIP, indicating the formation of molecular imprints as selective recognition sites in MIPs. Modeling allows deeper understanding of the adsorption thermodynamics. It clarifies whether increased adsorption is due to a stronger affinity or a higher density of molecular imprints. It shows that there are two types of adsorption processes (selective to molecular imprints and non-selective besides them) with different binding affinities are it has already clearly disclosed from Scatchard plots [33,34,35].

Both selective and non-selective adsorptions to MIP@AA were significantly larger than to MIP@MAA. The larger adsorption to molecular imprints of MIP@AA is due to two contributions: a larger density of molecular imprints and a higher affinity to them. Non-selective adsorption was identical on MIPs and NIPs of the same composition ($Q_{max,ns}$ and K_{ns} are identical). Non-selective adsorption was higher for AA-based materials than for MAA-based ones (Table 2). The higher affinity of AA-based molecular imprints is in agreement with the higher complexation constant of HA and AA in solution. The stronger association of HA and the functional monomer not only increases the binding affinity (K_s), but also the density of molecular imprints ($Q_{max,s}$). This supports the idea of the definite role of the pre-polymerization complex, although the mechanism by which it contributes to the formation of molecular imprints is not clearly explained.

4. Conclusion

The current study addresses the question on whether interactions between very strong acids and bases may allow for the formation of highly selective molecular imprints. It is shown that mixing strong acids and bases causes proton transfer from the acid to the base instead of developing hydrogen-bonded interactions. Suitable acid-base interactions that allow the formation of hydrogen bonds are those where the proton is shared between the two partners. The topic is illustrated by comparing the cases of the HA-MAA and the HA-AA pairs. ^{1}H NMR studies of interactions in solution have shown that the hydrogen-bonding interaction between HA and MAA is weaker than between HA and AA. The consequence is a higher performance of the AA-based MIP for selective binding of HA.

Notably, the adsorption experiments together with their thermodynamic modeling provided more detailed insights on the MIP@AA behavior. The higher hydrogen-bonding interactions of AA and HA caused both a higher affinity of HA to molecular imprints and a higher density of molecular imprints. The systematic use of methacrylic acid as a kind of 'universal' functional monomer may be reconsidered according to the present findings.

CRediT authorship contribution statement

Merymene Boukadida: Investigation, Data curation, Formal analysis, Writing – original draft. **Amira Anene:** Investigation, Methodology. **Najeh Jaoued-Grayaa:** Methodology, Validation. **Yves Chevalier:** Conceptualization, Validation, Supervision, Funding acquisition, Project administration, Writing – review & editing. **Souhaira Hbaieb:** Conceptualization, Validation, Supervision, Funding acquisition, Project administration, Writing – review & editing.

Declaration of Competing Interest

The authors declare that they have no known competing financial interests or personal relationships that could have appeared to influence the work reported in this paper.

Data availability

Data will be made available on request.

Acknowledgments

This work was supported by the "PHC Utique" program for French-Tunisian cooperation (project number 19G1204).

Appendix A. Supplementary data

Supplementary data to this article can be found online at https://doi.org/10.1016/j.colcom.2022.100669.

References

[1] B. Sellergren (Ed.), Molecularly Imprinted Polymers: Man-Made Mimics of Antibodies and their Application in Analytical Chemistry, Elsevier, 2000.

[2] A.G. Mayes, K. Mosbach, Molecularly imprinted polymers: useful materials for analytical chemistry? Trends Anal. Chem. 16 (1997) 321–332, https://doi.org/10.1016/S0165-9936(97)00037-X.

[3] C. Alvarez-Lorenzo, A. Concheiro (Eds.), Handbook of Molecularly Imprinted Polymers, Smithers Rapra, Shawbury, UK, 2013.

[4] T. Curk, J. Dobnikar, D. Frenkel, Rational design of molecularly imprinted polymers, Soft Matter 12 (2016) 35–44, https://doi.org/10.1039/c5sm02144h.

[5] B. Sellergren, M. Lepistó, K. Mosbach, Highly enantioselective and substrate-selective polymers obtained by molecular imprinting utilizing noncovalent interactions. NMR and chromatographic studies on the nature of recognition, J. Am. Chem. Soc. 110 (1988) 5853–5860, https://doi.org/10.1021/ja00225a041.

[6] P.U. Ashvin Iresh Fernando, M.W. Glasscott, G.K. Kosgei, J.S. Cobb, E.M. Alberts, C.G. Bresnahan, T.C. Schutt, G.W. George, L.C. Moores, Toward rational design of electrogenerated molecularly imprinted polymers (eMIPs): maximizing monomer/template affinity, ACS Appl. Polym. Mater. 3 (2021) 4523–4533, https://doi.org/10.1021/acsapm.1c00575.

[7] B. Sellergren, A.J. Hall, Fundamental aspects on the synthesis and characterisation of imprinted network polymers, in: B. Sellergren (Ed.), Molecularly Imprinted Polymers: Man-made Mimics of Antibodies and Their Application in Analytical Chemistry, Elsevier, 2000, pp. 29–39. Chap. 2.

[8] J.L. Urraca, A.J. Hall, M.C. Moreno-Bondi, B. Sellergren, A stoichiometric molecularly imprinted polymer for the class-selective recognition of antibiotics in aqueous media, Angew. Chem. Int. Ed. 45 (2006) 5158–5161, https://doi.org/10.1002/anie.200601636.

[9] M.V. Sullivan, S.R. Dennison, G. Archontis, S.M. Reddy, J.M. Hayes, Toward rational design of selective molecularly imprinted polymers (MIPs) for proteins: computational and experimental studies of acrylamide based polymers for myoglobin, J. Phys. Chem. B 123 (2019) 5432–5443, https://doi.org/10.1021/acs.jpcb.9b03091.

[10] F. Horemans, J. Alenus, E. Bongaers, A. Weustenraed, R. Thoelen, J. Duchateau, L. Lutsen, D. Vanderzande, P. Wagner, T.J. Cleij, MIP-based sensor platforms for the detection of histamine in the nano- and micromolar range in aqueous media, Sensors Actuators B Chem. 148 (2010) 392–398, https://doi.org/10.1016/j.snb.2010.05.003.

[11] X.N. Zhou, Y. Yu, S. Liu, S.L. Yan, Q.Z. Wang, J. Li, Preparation and recognized characteristic of histamine molecularly imprinted polymers, Adv. Mater. Res. 550–553 (2012) 780–786, https://doi.org/10.4028/www.scientific.net/AMR.550-553.780.

[12] A. Sahebnasagh, G. Karimi, S.A. Mohajeri, Preparation and evaluation of histamine imprinted polymer as a selective sorbent in molecularly imprinted solid-phase extraction coupled with high performance liquid chromatography analysis in canned fish, Food Anal. Methods 7 (2014) 1–8, https://doi.org/10.1007/s12161-013-9579-7.

[13] F. Holmes, F. Jones, Metal complexes of histamine and some structural analogues. Part I, J. Chem. Soc. (1960) 2398–2401, https://doi.org/10.1039/JR9600002398.

[14] V. Madhavan, N.N. Lichtin, E. Hayon, Protonation reactions of electron adducts of acrylamide derivatives. A pulse radiolytic-kinetic spectrophotometric study, J. Am. Chem. Soc. 97 (1975) 2989–2995, https://doi.org/10.1021/ja00844a013.

[15] B.L. Schottel, H.T. Chifotides, K.R. Dunbar, Anion-π interactions, Chem. Soc. Rev. 37 (2008) 68–83, https://doi.org/10.1039/B614208G.

[16] J. O'Mahony, A. Molinelli, K. Nolan, M.R. Smyth, B. Mizaikoff, Towards the rational development of molecularly imprinted polymers: ^{1}H NMR studies on hydrophobicity and ion-pair interactions as driving forces for selectivity, Biosens. Bioelectron. 20 (2005) 1884–1893, https://doi.org/10.1016/j.bios.2004.07.036.

[17] U. Athikomrattanakul, M. Katterle, N. Gajovic-Eichelmann, F.W. Scheller, Development of molecularly imprinted polymers for the binding of nitrofurantoin, Biosens. Bioelectron. 25 (2009) 82–87, https://doi.org/10.1016/j.bios.2009.06.003.

[18] A. Noomane, S. Hbaieb, M.-A. Bolzinger, S. Briançon, Y. Chevalier, R. Kalfat, Effectiveness of grafting modes of methoxycinnamate sunscreen onto silica particles, Coll. Surf. A Physicochem. Eng. Asp. 441 (2014) 653–663, https://doi.org/10.1016/j.colsurfa.2013.10.029.

[19] A. El Harrak, G. Carrot, J. Oberdisse, J. Jestin, F. Boué, Atom transfer radical polymerization from silica nanoparticles using the 'grafting from' method and structural study via small-angle neutron scattering, Polymer 46 (2005) 1095–1104, https://doi.org/10.1016/j.polymer.2004.11.046.

[20] H.-S. Jung, D.-S. Moon, J.-K. Lee, Quantitative analysis and efficient surface modification of silica nanoparticles, J. Nanomater. 2012 (2012) 1–8, https://doi.org/10.1155/2012/593471.

[21] F. Ulatowski, K. Dąbrowa, T. Bałakier, J. Jurczak, Recognizing the limited applicability of job plots in studying host–guest interactions in supramolecular chemistry, J. Organomet. Chem. 81 (2016) 1746–1756, https://doi.org/10.1021/acs.joc.5b02909.

[22] J.S. Renny, L.L. Tomasevich, E.H. Tallmadge, D.B. Collum, Method of continuous variations: applications of job plots to the study of molecular associations in organometallic chemistry, Angew. Chem. Int. Ed. 52 (2013) 11998–12013, https://doi.org/10.1002/anie.201304157.

[23] M. Dimitrijevic, S. Stefanovic, N. Karabasil, D. Vasilev, N. Cobanovic, N. Ilic, V. Djordjevic, UPLC-MS/MS determination of histamine levels in canned fish collected from Belgrade retail markets, Meat Technol. 57 (2016) 47–56. http://www.journalmeattechnology.com/index.php/meat_technology/article/view/38.

[24] C. Dong, H. Shi, Y. Han, Y. Yang, R. Wang, J. Men, Molecularly imprinted polymers by the surface imprinting technique, Eur. Polym. J. 145 (2021), 110231, https://doi.org/10.1016/j.eurpolymj.2020.110231.

[25] I. Lacík, L. Učňová, S. Kukučková, M. Buback, P. Hesse, S. Beuermann, Propagation rate coefficient of free-radical polymerization of partially and fully ionized methacrylic acid in aqueous solution, Macromolecules 42 (2009) 7753–7761, https://doi.org/10.1021/ma9013516.

[26] I. Lacík, A. Chovancová, L. Uhelská, C. Preusser, R.A. Hutchinson, M. Buback, PLP-SEC studies into the propagation rate coefficient of acrylamide radical polymerization in aqueous solution, Macromolecules 49 (2016) 3244–3253, https://doi.org/10.1021/acs.macromol.6b00526.

[27] M. Thommes, K. Kaneko, A.V. Neimark, J.P. Olivier, F. Rodriguez-Reinoso, J. Rouquerol, K.S.W. Sing, Physisorption of gases, with special reference to the evaluation of surface area and pore size distribution (IUPAC technical report), Pure Appl. Chem. 87 (2015) 1051–1069, https://doi.org/10.1515/pac-2014-1117.

[28] K. Hirose, A practical guide for the determination of binding constants, J. Incl. Phenom. Macrocycl. Chem. 39 (2001) 193–209, https://doi.org/10.1023/A:1011117412693.

[29] F. Ulatowski, K. Dąbrowa, T. Bałakier, J. Jurczak, Recognizing the limited applicability of Job Plots in studying host–guest interactions in supramolecular chemistry, J. Organomet. Chem. 81 (2016) 1746–1756, https://doi.org/10.1021/acs.joc.5b02909.

[30] C. Ayadi, A. Anene, R. Kalfat, Y. Chevalier, S. Hbaieb, Molecular imprints frozen by strong intermolecular interactions in place of cross-linking, Chem. Eur. J. 27 (2021) 2175–2183, https://doi.org/10.1002/chem.202004580.

[31] I. Langmuir, The adsorption of gases on plane surfaces of glass, mica and platinum, J. Am. Chem. Soc. 40 (1918) 1361–1403, https://doi.org/10.1021/ja02242a004.

[32] M. Volmer, Thermodynamische Folgerungen ans der Zustandsgleichung für adsorbierte Stoffe, Z. Phys. Chem. 115 (1925) 253–260, https://doi.org/10.1515/zpch-1925-11519.

[33] B. Zu, G. Pan, X. Guo, Y. Zhang, H. Zhang, Preparation of molecularly imprinted polymer microspheres via atom transfer radical precipitation polymerization, J. Polym. Sci., A: Polym. Chem. 47 (2009) 3257–3270, https://doi.org/10.1002/pola.23389.

[34] B. Zu, Y. Zhang, X. Guo, H. Zhang, Preparation of molecularly imprinted polymers via atom transfer radical "bulk" polymerization, J. Polym. Sci., A: Polym. Chem. 48 (2010) 532–541, https://doi.org/10.1002/pola.23750.

[35] Y. Ma, G. Pan, Y. Zhang, X. Guo, H. Zhang, Comparative study of the molecularly imprinted polymers prepared by reversible addition–fragmentation chain transfer "bulk" polymerization and traditional radical "bulk" polymerization, J. Mol. Recognit. 26 (2013) 240–251, https://doi.org/10.1002/jmr.2267.

SUPPORTING INFORMATION

Choice of the functional monomer of molecularly imprinted polymers: Does it rely on strong acid-base or hydrogen bonding interactions ?

Merymene Boukadida[a,b], Amira Anene[c], Najeh Jaoued-Grayaa[c], Yves Chevalier[a*], Souhaira Hbaieb[b*]

[a] Laboratoire d'Automatique, de Génie des Procédés et de Génie Pharmaceutique, Université de Lyon 1, UMR 5007 CNRS, 69622 Villeurbanne Cedex, France.
[b] Laboratoire de Recherche: Caractérisations, Applications et Modélisation de Matériaux, Université de Tunis El Manar, Faculté des Sciences de Tunis, Campus universitaire El Manar, Tunisia.
[c] Unité Spécialisée de développement des techniques analytiques, Institut National de Recherche et d'Analyse Physico-chimique, Biotechpole Sidi-Thabet, 2020 Ariana, Tunisia.

S.1. Characterization of the modified silica

The IR spectrum (Fig. S1) of modified silica SiO_2(APTES-MA) shows the presence of a strong absorption band of the SiO_2 group as well as the typical bands resulting from chemical grafting: those of the coupling agent (aminosilane) and those arising from the addition of methacryloyl chloride. Since only a part of surface silanols are converted by the grafting reaction, the residual silanols exhibit a specific low-intensity band related to the ν_{Si-OH} vibration at 3100 cm^{-1}. A distinctive band corresponding to the $\nu_{C=O}$ vibration of a secondary amide at 1700 cm^{-1}. The elongation bands overlap at 1600 cm^{-1}, corresponding to the $\nu_{C=C}$ and ν_{C-N} vibrations. The ν_{Si-C} vibration has a significant characteristic band at about 1250 cm^{-1}. A distinctive band corresponding to the elongation vibration of Si–O–Si was observed at 1025 cm^{-1}. A secondary amide N–H deformation vibration is observed at 1500 cm^{-1}. The presence of vibrations ranging from 2960 to 2850 cm^{-1} of CH_2 and CH_3 elongations proves the presence of organic substances.

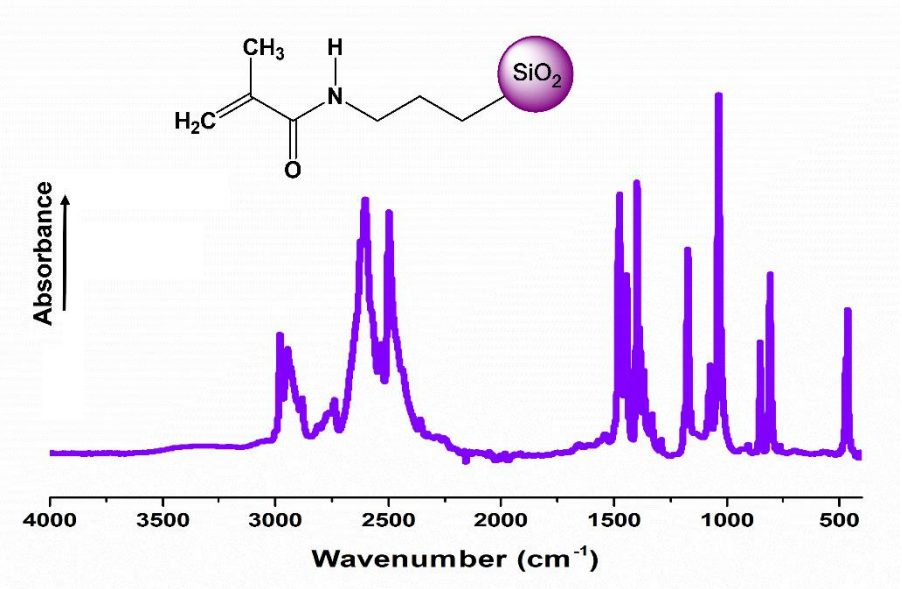

Figure S1. IR spectrum of SiO_2(APTES-MA).

The thermal analysis of SiO_2(APTES-MA) is shown in Fig. S2. The presence of moisture and the condensation of unreacted Si–OEt groups explains a first mass loss at 200 °C. A second mass loss was recorded between 350 and 600 °C, corresponding to the progressive degradation of the organic grafts on the silica surface.

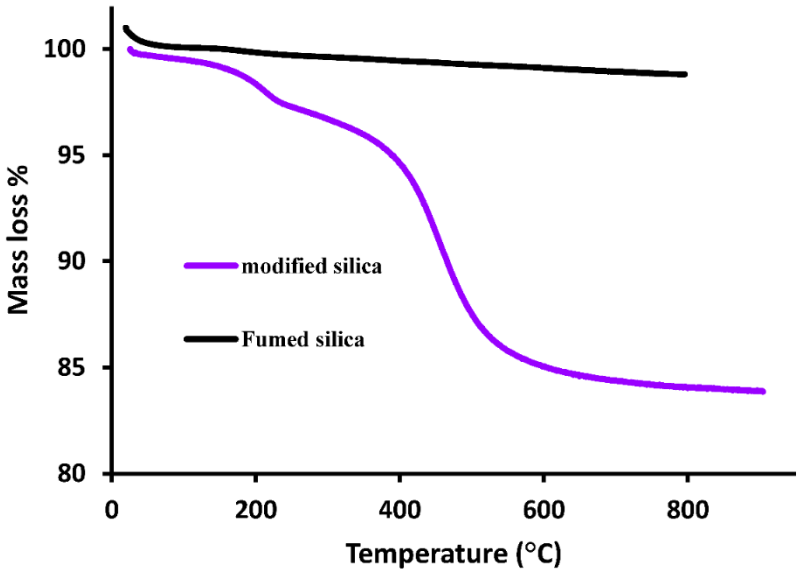

Figure S2. Thermogravimetric analysis of SiO_2(APTES-MA).

The graft mass loss (APTES-MA) between 350 °C and 600 °C was used to calculate the grafting density using the following equation:

$$\mathcal{T}(\mu\text{mol}\cdot\text{m}^{-2}) = \frac{\frac{m(\text{APTES-MA})}{100-m(\text{SiO}_2\text{-APTES-MA})}\times 100 - m(\text{SiO}_2)}{M(\text{APTES-MA})\times A_{\text{sp}}\times 100}\times 10^6 \quad \text{(S1)}$$

where m(SiO_2-APTES-MA) is the mass loss difference between the grafted organic part m(APTES-MA) = 14.20% (Table S1) and the fumed silica m(SiO_2) = 0.9%. Taking $SiC_7H_{12}N$ as the chemical formula of the grafts, their graft molar mass is M(APTES-MA) = 126 g·mol^{-1}. A_{sp} is the specific surface area of silica (200 m^2·g^{-1}).

Elemental analyses (EA) of carbon and nitrogen provide supplementary estimates of the grafting density using Eqs S2 and S3.

$$\mathcal{T}(\mu\text{mol}\cdot\text{m}^{-2}) = \frac{1}{A_{\text{sp}}}\frac{1}{\frac{100\times 12\times n_{\text{C}}}{\%\text{C}}-1}\times 10^6 \quad \text{(S2)}$$

$$\mathcal{T}(\mu\text{mol}\cdot\text{m}^{-2}) = \frac{1}{A_{\text{sp}}}\frac{1}{\frac{100\times 12\times n_{\text{N}}}{\%\text{N}}-1}\times 10^6 \quad \text{(S3)}$$

where n_C and n_N are the numbers of carbon and nitrogen atoms in the graft, respectively; Asp is the specific surface area of silica (200 m^2·g^{-1}); %C and %N are the percentages of carbon and nitrogen obtained in elemental analyses.

The grafting densities found from elemental analyses were in accordance with those determined by TGA (Table S1).

Table S1. Surface densities of methacryloyl grafts from TGA and elemental analyses.

Material	Elemental analysis (%)		Surface density (µmol·m^{-2}) from EA		from TGA
	C	N	C	N	
SiO_2(APTES-MA)	10.80	1.75	6.44	6.26	6.21

S.2. Characterization of the of MIP and NIP materials

The thermogravimetric analysis records for the imprinted and non-imprinted materials (Fig. S3) revealed a much larger mass loss between 250 and 450 °C compared to the modified silica, indicating that the polymerization reaction was successful. The thermograms show that the materials have an excellent thermal resistance. The mass losses are equal to the polymer contents. As expected, the polymer contents of the MIP and NIP were identical, indicating that HA was extracted to completion from the polymer matrix. The polymer contents was ~20% larger for AA-based than MAA-based materials (Table S2), indicating that the active polymer layer of MIP@AA was slightly thicker than for MIP@MAA. A slight enhanced density of molecular imprints may be expected in MIP@AA on this basis.

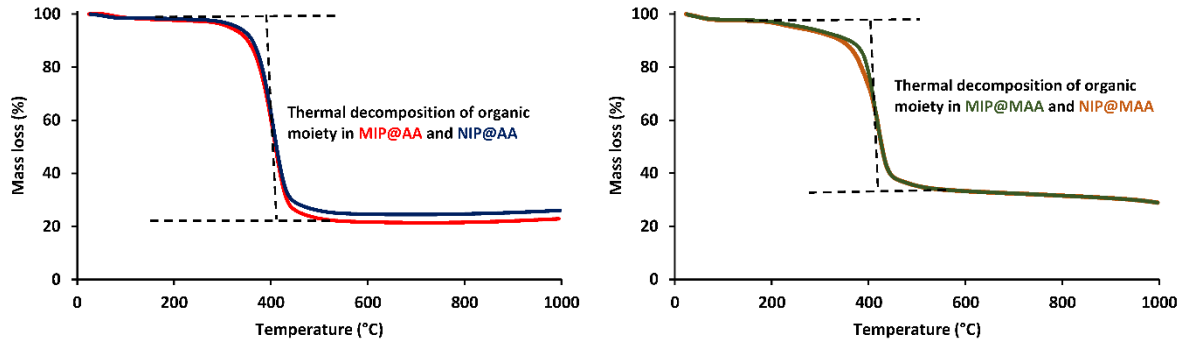

Figure S3. Superimposition of the thermograms of the two synthesized MIPs and NIPs.

Table S2. Mass losses of the MIPs and NIPs.

Polymer	Mass loss (%)
MIP@MAA	53.1
NIP@MAA	53.2
MIP@AA	67.7
NIP@AA	67.9

BET nitrogen gas adsorption experiments (Fig. S4) provide the specific surface area of the solid powders, and the BJH approach provides the pore size distribution and total volume of the mesopores.

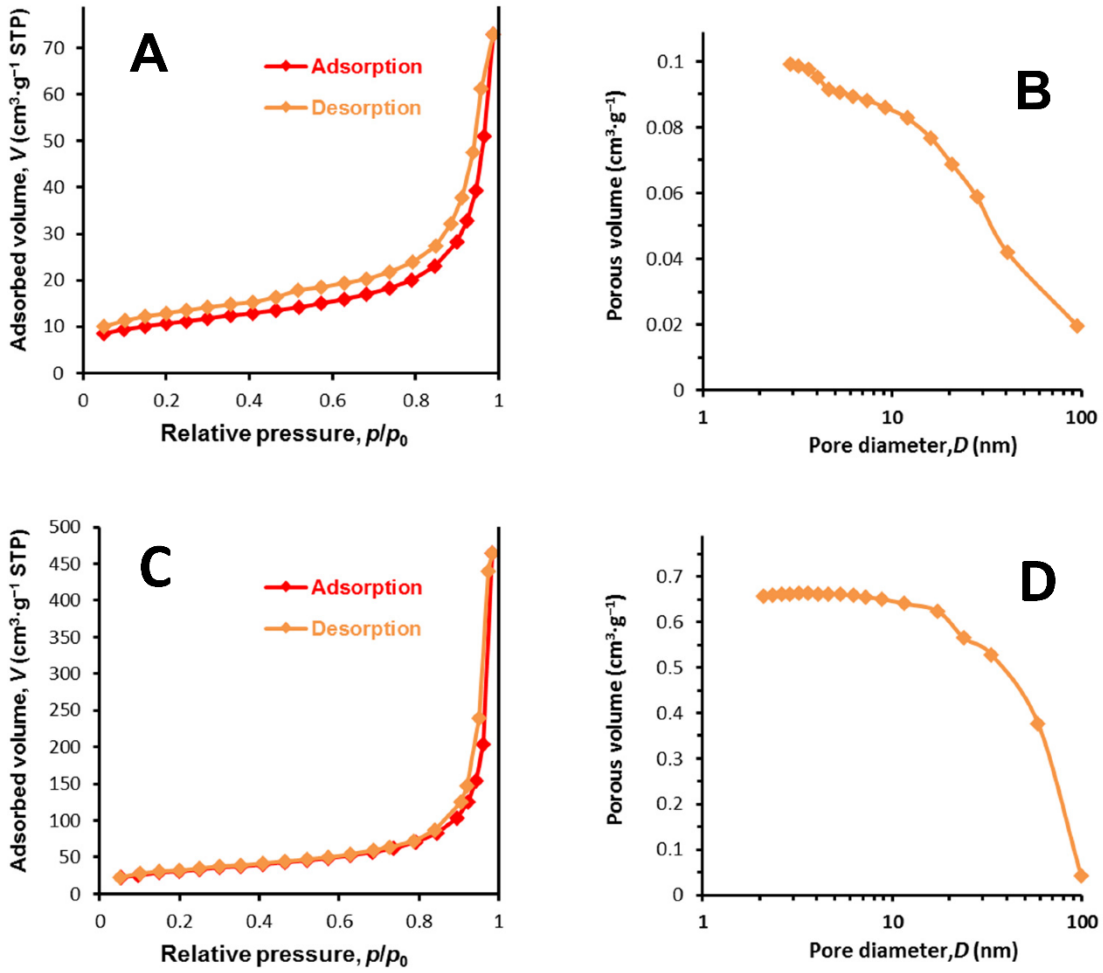

Figure S4. Nitrogen gas adsorption (red) and desorption (orange) isotherms at 77 K on the MIP@AA material (A) and the MIP@MAA material (C). Application of the BJH approach to the desorption branch to assess the distribution of the mesoporous volume for the MIP@AA (B) and MIP@MAA (D).

S.3. NMR studies of the pre-polymerization complexes

The stoichiometry and complexation constant of the HA-monomer complex species have been determined by measurements of ^{1}H NMR chemical shifts differences $\Delta\delta$ between mixed HA-monomer solutions and solutions of pure compounds (either HA or monomer). Typical spectra are shown in Figs S5 and S6.

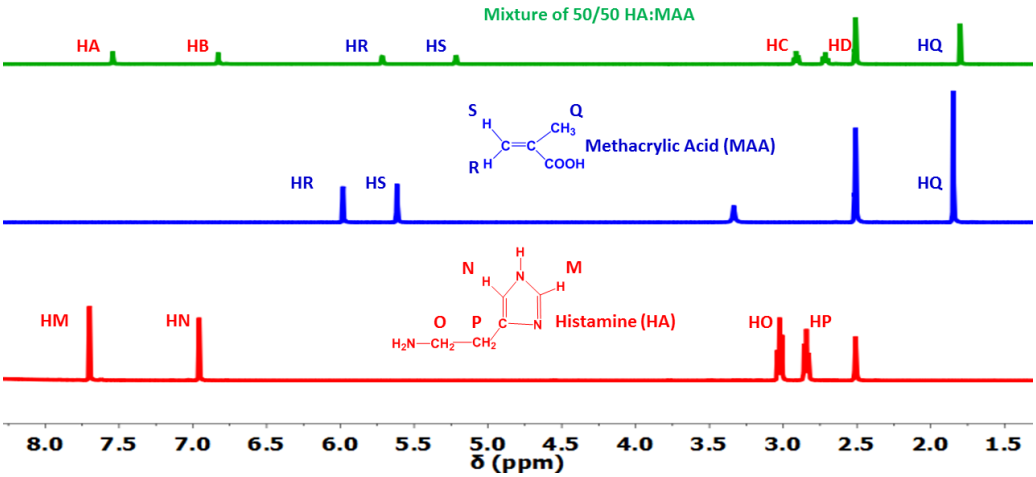

Figure S5. ^{1}H NMR spectra of pure MAA and HA, and their equimolar mixture.

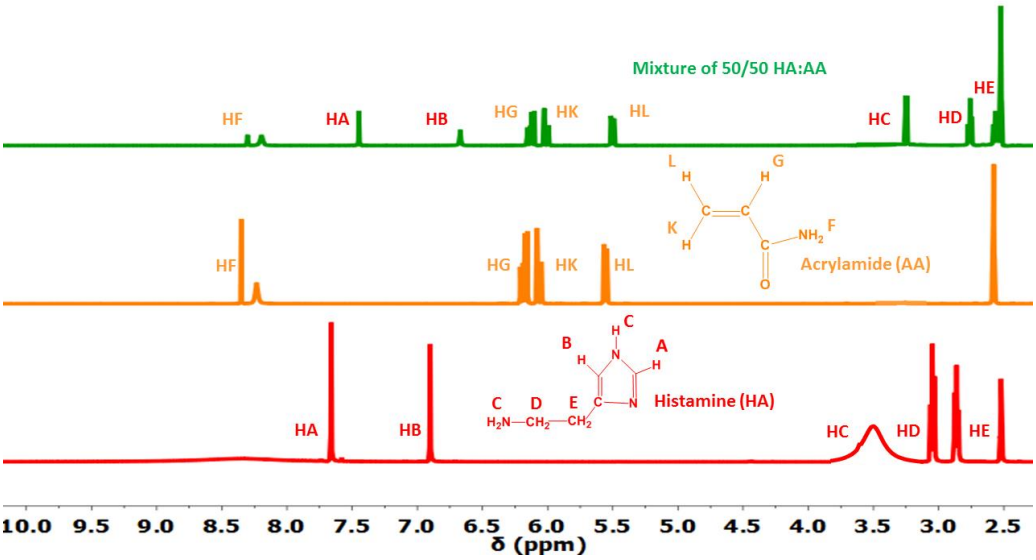

Figure S6. ^{1}H NMR spectra of pure MAA and HA, and their equimolar mixture.

The compositions of the mixtures were those used in the Job method. The mole fraction of HA r = [HA]/([HA] + [monomer] was varied while keeping constant the total concentration [HA] + [monomer]. Job plots of $r\Delta\delta$ vs r of all ^{1}H NMR lines of HA and of $(1-r)\Delta\delta$ vs $1-r$ of the lines of the monomer (MAA or AA) are given in Figs S7 to S10. The maximum of $r\Delta\delta$ (for HA lines) and $(1-r)\Delta\delta$ (for monomer lines) was located at r = 0.5 in all instances, showing that the stoichiometry of the complexes is 1:1. The complexation constants for the 1:1 complexes were determined by fitting the theoretical Job plots to the experimental data. The formation of the 1:1 complex (C) between HA and the monomer (M) is described by the classical equilibrium

$$HA + M \leftrightarrows C \quad (S4)$$

The equilibrium is expressed by the complexation constant K of the law of mass action

$$K = \frac{[C]}{[HA][M]} \quad (S5)$$

As a result, HA exists in the two free and complexed forms; and the monomer M also does. The calculation of [HA], [M], and [C] was done by solving the system of the 3 equations, Eqs S5, S6 and S7

$$\text{Balance of HA: } [HA]_{tot} = [HA] + [C] \quad (S6)$$

$$\text{Balance of M: } [M]_{tot} = [M] + [C] \quad (S7)$$

that yields the 2nd degree equation of unknown parameter [C]

$$[C]^2 - [C]\left([HA]_{tot} + [M]_{tot} + \frac{1}{K}\right) + [HA]_{tot}[M]_{tot} = 0 \quad (S8)$$

whose solution is

$$[C] = \frac{\left([HA]_{tot}+[M]_{tot}+\frac{1}{K}\right) - \sqrt{\left([HA]_{tot}+[M]_{tot}+\frac{1}{K}\right)^2 - 4[HA]_{tot}[M]_{tot}}}{2} \quad (S9)$$

For the protons of HA under the fast exchange limit, the chemical shift (δ) is the average of the chemical shifts of free HA (δ_{HA}) and C (δ_C) weighted by their mole fractions (x_{HA} and x_C)

$$\delta = x_{HA}\delta_{HA} + x_C\delta_C = \frac{[HA]}{[HA]_{tot}}\delta_{HA} + \frac{[C]}{[HA]_{tot}}\delta_C \quad (S10)$$

The same type of equation holds for the protons of M

$$\delta = x_M\delta_M + x_C\delta_C = \frac{[M]}{[M]_{tot}}\delta_M + \frac{[C]}{[M]_{tot}}\delta_C \quad (S11)$$

The complexation constant and chemical shifts of the NMR lines of the complex were adjusted such as to minimize the average relative error function (*ARE*) for *n* data points and *p* adjustable parameters) using the non-linear GRG algorithm of the Excel Solver:

$$ARE = \frac{1}{n-p}\sum_{i=1}^{n}\left|\frac{Q_{exp}-Q_{calc}}{Q_{exp}}\right| \quad (S12)$$

Figs S7 and S8, and Figs S9 and S10 show the experimental data (dots) together with the best theoretical fits (solid lines) for the HA-AA and HA-MAA systems, respectively.

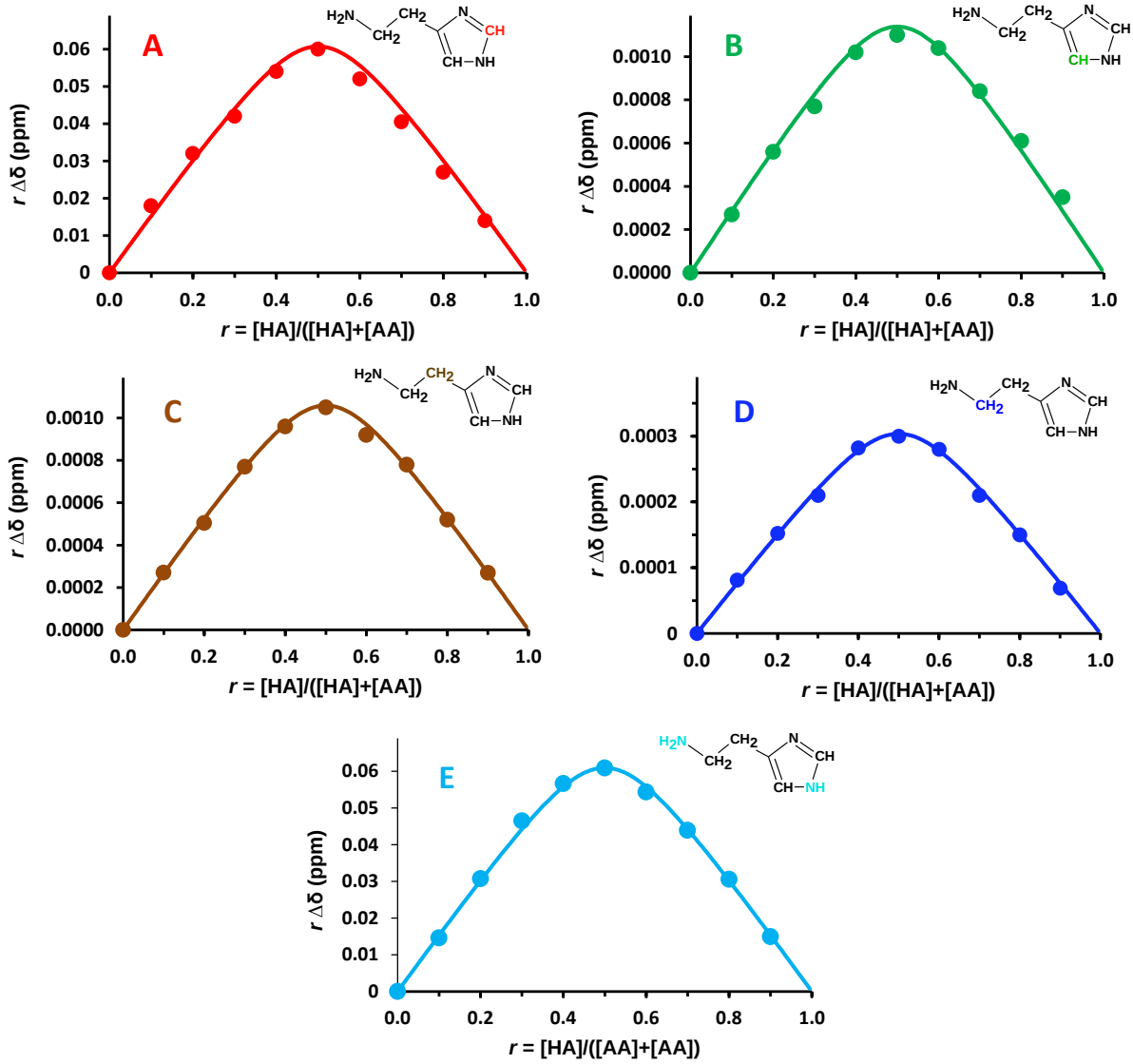

Figure S7. Job plots for the chemical shifts of HA protons (A, B, C, D, E) in the HA-AA mixed samples. The solid line is the best fit to the experimental data.

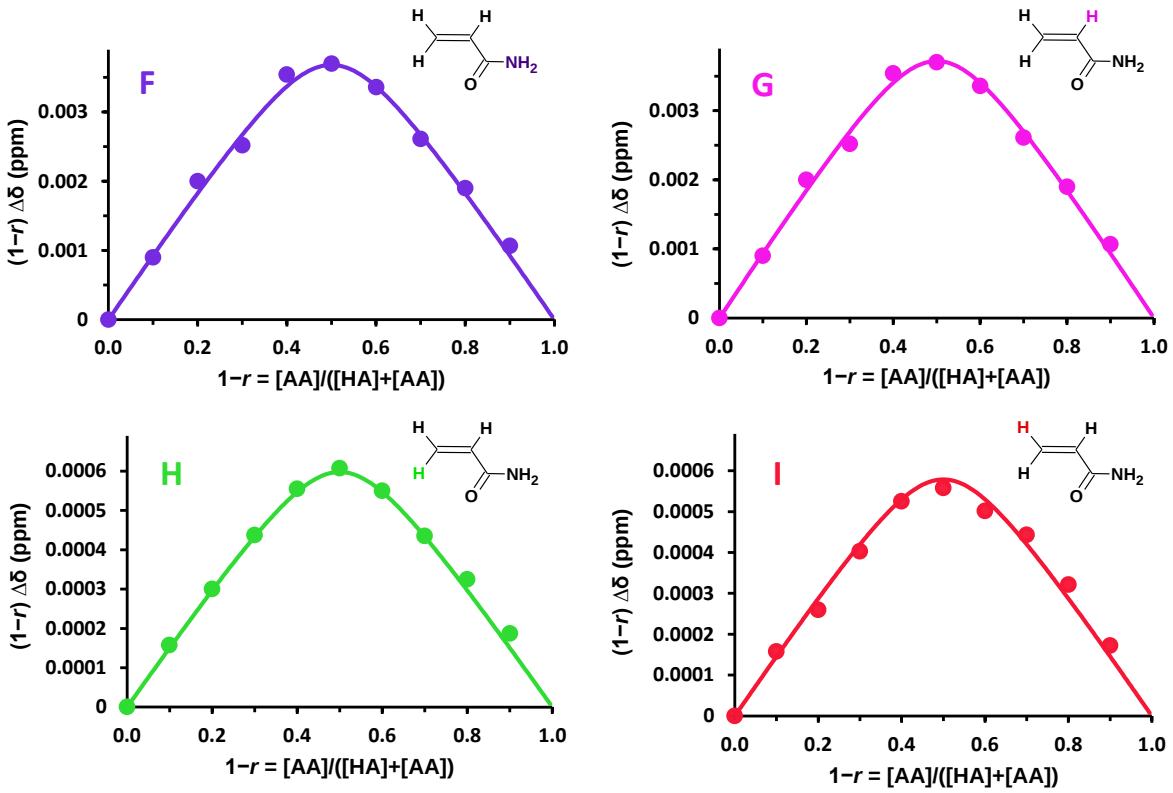

Figure S8. Job plots for the chemical shifts of AA protons (F, G, H, I) in the HA-AA mixed samples. The solid line is the best fit to the experimental data.

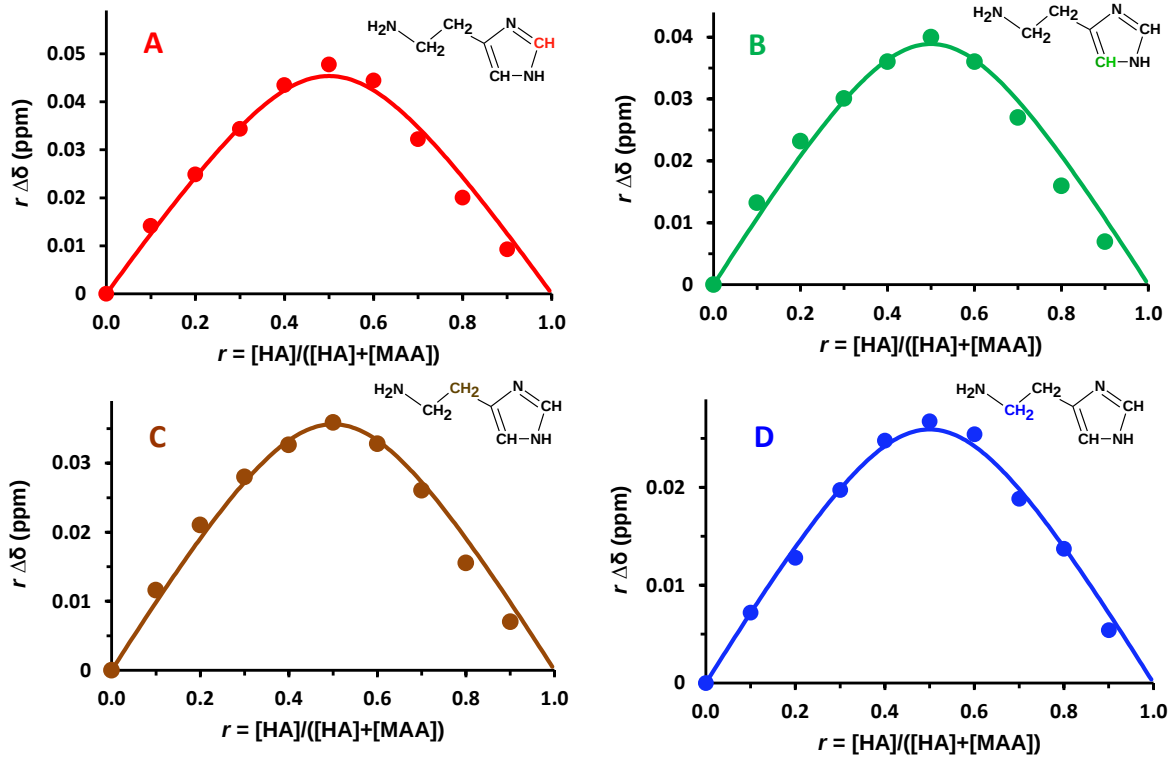

Figure S9. Job plots for the chemical shifts of HA protons (A, B, C, D) in the HA-MAA mixed samples. The solid line is the best fit to the experimental data.

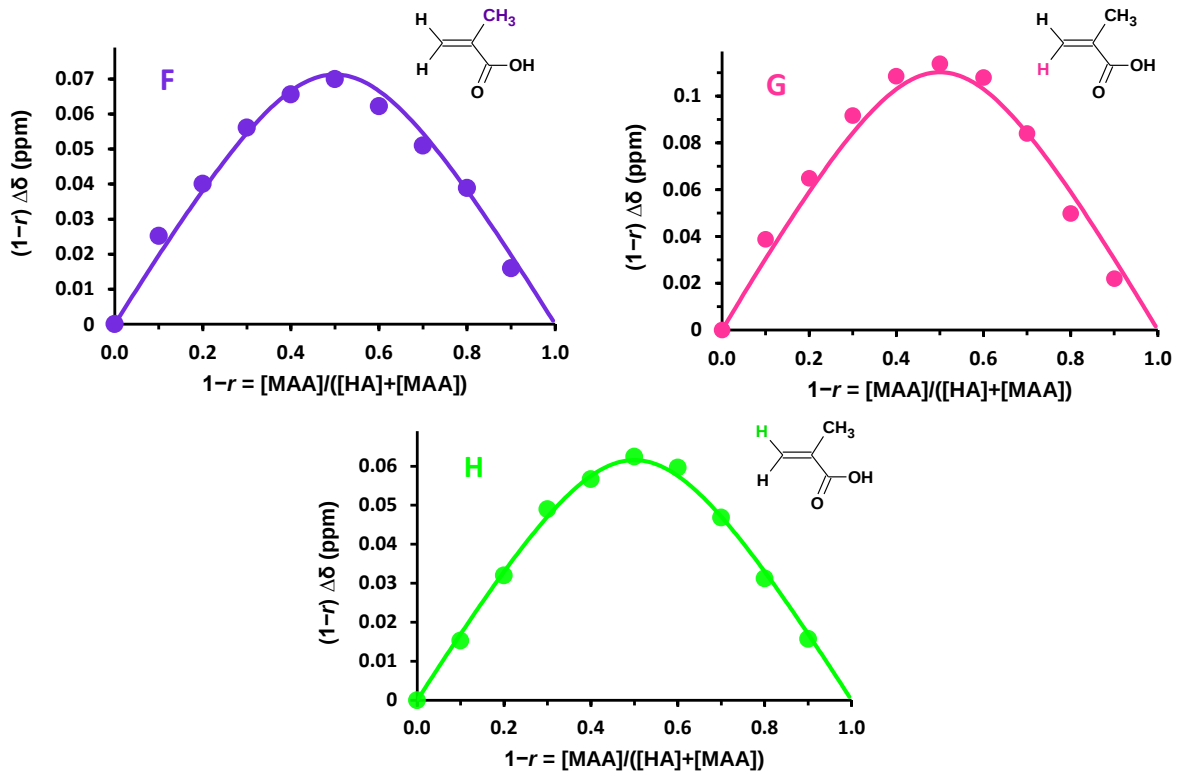

Figure S10. Job plots for the chemical shifts of MAA protons (F, G, H) the HA-MAA mixed samples. The solid line is the best fit to the experimental data.

S.4. Calibration curves for histamine analysis by LC-MS

Two HA stock solutions (100 mg·L^{-1} and 300 mg·L^{-1}) were made in deionized water and kept at 4 °C. Working standard solutions in the ranges of 0.5–10 ppm and 15–300 ppm were prepared by diluting stock solutions to measure the two calibration curves. All solutions were filtered through a 0.2 µm Nylon syringe filter before being analyzed by LC-MS. The HA peak was detected 2.049 min after the injection of the HA solutions as seen in the chromatogram in Fig. S11. The HA calibration curves exhibit high linearity with $R^2 > 0.999$ (Fig. S12).

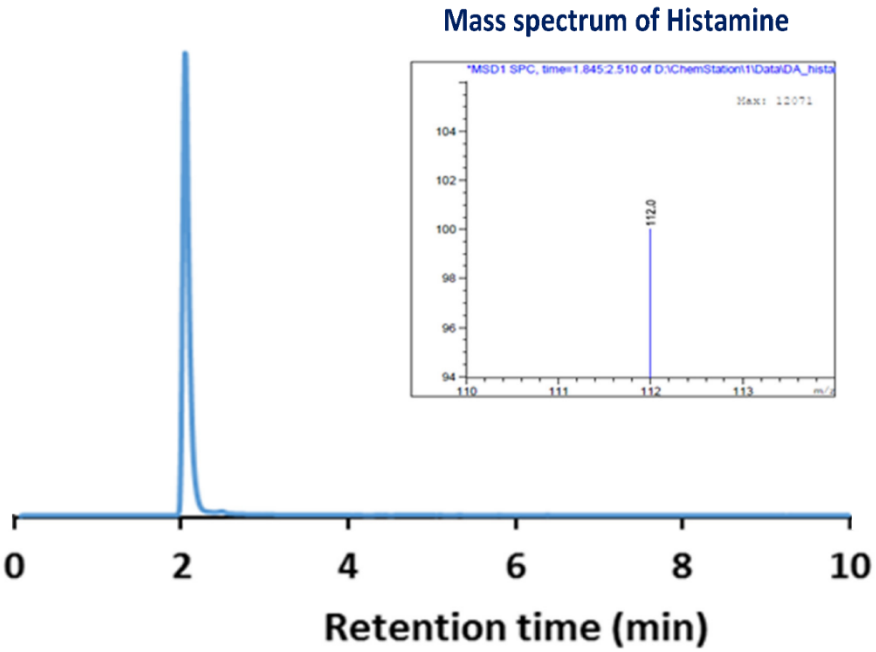

Figure S11. Chromatogram of histamine.

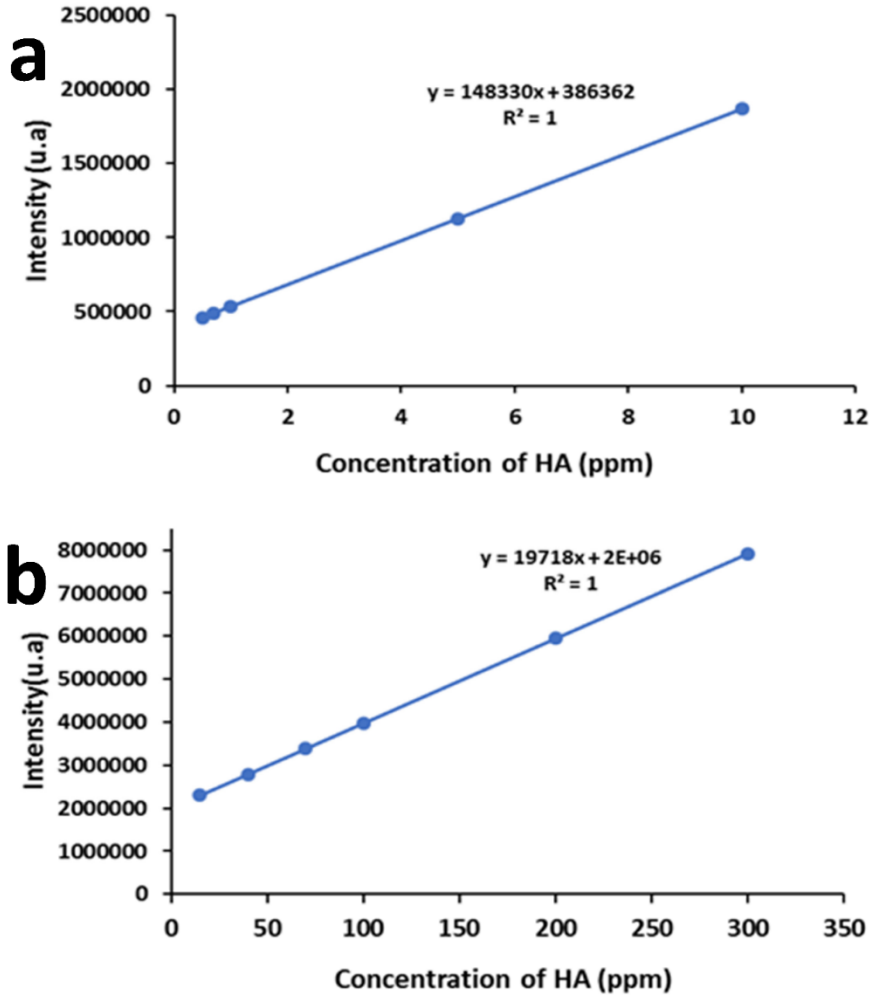

Figure S12. Calibration curves for histamine from 0.5–10 ppm (a) and 15–300 ppm (b).